Direct Immobilization of Native Yeast Iso-1 Cytochrome *c* on Bare Gold: Fast Electron Relay to Redox Enzymes and Zeptomole Protein-Film Voltammetry

Hendrik A. Heering,*[†,‡] Frank G. M. Wiertz,[†] Cees Dekker,[‡] and Simon de Vries[†]

Contribution from the Department of Biotechnology, Faculty of Applied Sciences, Delft University of Technology, Julianalaan 67, 2628 BC Delft, The Netherlands, and Kavli Institute of Nanoscience, Faculty of Applied Sciences, Delft University of Technology, Lorentzweg 1, 2628 CJ Delft, The Netherlands

Received June 3, 2004; E-mail: h.a.heering@tnw.tudelft.nl

Abstract: Cyclic voltammetry shows that yeast iso-1-cytochrome *c* (YCC), chemisorbed on a bare gold electrode via Cys102, exhibits fast, reversible interfacial electron transfer ($k_0 = 1.8 \times 10^3$ s^{-1}) and retains its native functionality. Vectorially immobilized YCC relays electrons to yeast cytochrome *c* peroxidase, and to both cytochrome cd_1 nitrite reductase (NIR) and nitric oxide reductase from *Paracoccus denitrificans*, thereby revealing the mechanistic properties of these enzymes. On a microelectrode, we measured nitrite turnover by ~80 zmol (49 000 molecules) of NIR, coadsorbed on 0.65 amol (390 000 molecules) of YCC.

Introduction

Protein electrochemistry has become a powerful tool, both to study redox enzymes and to make sensitive biosensor devices.[1-6] For optimal control of the oxidation state of the cofactors and efficient relay of electrons to the active site, fast interfacial electron transfer is a prerequisite. Often, however, the cofactors cannot make efficient contact with the electrode surface, or substrate access is blocked by the electrode. Because small redox proteins like azurin, ferredoxin, and cytochromes are natural electron shuttles for redox enzymes and readily exchange electrons with solid electrodes, these can be used as mediators.[7-9] To reveal the properties of the enzyme under study, fast electron relay by the mediating protein is required.

Diffusion limitations can be minimized by immobilizing the mediator, with the correct orientation for electron exchange with both the electrode and the enzyme. Although an orientation with the cofactor toward the electrode surface favors interfacial electron transfer, the same side is usually involved in docking of enzymes. Moreover, close proximity of the cofactor to the electrode can significantly modify its properties.[10,11] One solution is a flexible tether to confine the protein to the surface, allowing reorientation for fast electron exchange with both the electrode[12] and the enzyme.[8] However, such an arrangement will considerably attenuate the overall electron shuttling rate.

† Department of Biotechnology.
‡ Kavli Institute of Nanoscience.

(1) (a) Armstrong, F. A.; Wilson, G. S. *Electrochim. Acta* **2000**, *45*, 2623−2645. (b) Fedurco, M. *Coord. Chem. Rev.* **2000**, *209*, 263−331. (c) Willner, I.; Katz, E. *Angew. Chem., Int. Ed.* **2000**, *39*, 1180−1218. (d) Chaki, N. K.; Vijayamohanan, K. *Biosens. Bioelectron.* **2002**, *17*, 1−12. (e) Zu, Y. B.; Shannon, R. J.; Hirst, J. *J. Am. Chem. Soc.* **2003**, *125*, 6020−6021.
(2) (a) Armstrong, F. A.; Heering, H. A.; Hirst, J. *Chem. Soc. Rev.* **1997**, *26*, 169−179. (b) Anderson, L. J.; Richardson, D. J.; Butt, J. N. *Faraday Discuss.* **2000**, *116*, 155−169. (c) Angove, H. C.; Cole, J. A.; Richardson, D. J.; Butt, J. N. *J. Biol. Chem.* **2002**, *277*, 23374−23381. (d) Armstrong, F. A. *J. Chem. Soc., Dalton Trans.* **2002**, 661−671. (e) Elliott, S. J.; Léger, C.; Pershad, H. R.; Hirst, J.; Heffron, K.; Ginet, N.; Blasco, F.; Rothery, R. A.; Weiner, J. H.; Armstrong, F. A. *Biochim. Biophys. Acta* **2002**, *1555*, 54−59. (f) Leger, C.; Elliott, S. J.; Hoke, K. R.; Jeuken, L. J. C.; Jones, A. K.; Armstrong, F. A. *Biochemistry* **2003**, *42*, 8653−8662. (g) Liu, H. H.; Pang, D. W. *Prog. Chem.* **2002**, *14*, 425−432. (h) Elliott, S. J.; Hoke, K. R.; Heffron, K.; Palak, M.; Rothery, R. A.; Weiner, J. H.; Armstrong, F. A. *Biochemistry* **2004**, *43*, 799−807. (i) Frangioni, B.; Arnoux, P.; Sabaty, M.; Pignol, D.; Bertrand, P.; Guigliarelli, B.; Léger, C. *J. Am. Chem. Soc.* **2004**, *126*, 1328−1329.
(3) Heering, H. A.; Hirst, J.; Armstrong, F. A. *J. Phys. Chem. B* **1998**, *102*, 6889−6902.
(4) Scott, D. L.; Paddock, R. M.; Bowden, E. F. *J. Electroanal. Chem.* **1992**, *341*, 307−321.
(5) Mondal, M. S.; Fuller, H. A.; Armstrong, F. A. *J. Am. Chem. Soc.* **1996**, *118*, 263−264.
(6) Mondal, M. S.; Goodin, D. B.; Armstrong, F. A. *J. Am. Chem. Soc.* **1998**, *120*, 6270−6276.

(7) (a) Moreno, C.; Franco, R.; Moura, I.; Legall, J.; Moura, J. J. G. *Eur. J. Biochem.* **1993**, *217*, 981−989. (b) Amine, A.; Deni, J.; Kauffmann, J. M. *Bioelectrochem. Bioenerg.* **1994**, *34*, 123−128. (c) Verhagen, M. F. J. M.; Wolbert, R. B. G.; Hagen, W. R. *Eur. J. Biochem.* **1994**, *221*, 821−829. (d) Willner, I.; Katz, E.; Willner, B.; Blonder, R.; HelegShabtai, V.; Buckmann, A. F. *Biosens. Bioelectron.* **1997**, *12*, 337−356. (e) Jin, W.; Wollenberger, U.; Kärgel, E.; Schunck, W.-H.; Scheller, F. W. *J. Electroanal. Chem.* **1997**, *433*, 135−139. (f) Abass, A. K.; Hart, J. P.; Cowell, D. *Sens. Actuators, B* **2000**, *62*, 148−153. (g) Fridman, V.; Wollenberger, U.; Bogdanovskaya, V.; Lisdat, F.; Ruzgas, T.; Lindgren, A.; Gorton, L.; Scheller, F. W. *Biochem. Soc. Trans.* **2000**, *28*, 63−70. (h) Wirtz, M.; Klucik, J.; Rivera, M. *J. Am. Chem. Soc.* **2000**, *122*, 1047−1056. (i) Liu, H.; Hill, H. A. O.; Chapman, S. K. *J. Electroanal. Chem.* **2001**, *500*, 598−603. (j) Lopes, H.; Besson, S.; Moura, I.; Moura, J. J. G. *J. Biol. Inorg. Chem.* **2001**, *6*, 55−62. (k) Takagi, K.; Yamamoto, K.; Kano, K.; Ikeda, T. *Eur. J. Biochem.* **2001**, *268*, 470−476. (l) Lojou, E.; Cutruzzola, F.; Tegoni, M.; Bianco, P. *Electrochim. Acta* **2003**, *48*, 1055−1064. (m) Okuda, J.; Wakai, J.; Yuhashi, N.; Sode, K. *Biosens. Bioelectron.* **2003**, *18*, 699−704.
(8) Pardo-Yissar, V.; Katz, E.; Willner, I.; Kotlyar, A. B.; Sanders, C.; Lill, H. *Faraday Discuss.* **2000**, *116*, 119−134.
(9) Haas, A. S.; Pilloud, D. L.; Reddy, K. S.; Babcock, G. T.; Moser, C. C.; Blasie, J. K.; Dutton, P. L. *J. Phys. Chem. B* **2001**, *105*, 11351−11362.
(10) (a) Döpner, S.; Hildebrandt, P.; Rosell, F. I.; Mauk, A. G. *J. Am. Chem. Soc.* **1998**, *120*, 11246−11255. (b) Chen, X. X.; Ferrigno, R.; Yang, J.; Whitesides, G. A. *Langmuir* **2002**, *18*, 7009−7015. (c) Wackerbarth, H.; Hildebrandt, P. *ChemPhysChem* **2003**, *4*, 714−724.
(11) (a) Hirota, S.; Hayamizu, K.; Endo, M.; Hibino, T.; Takabe, T.; Kohzuma, T.; Yamauchi, O. *J. Am. Chem. Soc.* **1998**, *120*, 8177−8183. (b) Rivera, M.; Seetharaman, R.; Girdhar, D.; Wirtz, M.; Zhang, X. J.; Wang, X. Q.; White, S. *Biochemistry* **1998**, *37*, 1485−1494. (c) Johnson, D. L.; Maxwell, C. J.; Losic, D.; Shapter, J. G.; Martin, L. L. *Bioelectrochem.* **2002**, *58*, 137−147.

Iso-1-cytochrome *c* from bakers yeast (*Saccharomyces cerevisiae*),YCC, is of particular interest because it contains a unique surface cysteine residue. Notably, this Cys102 is located next to the surface-exposed C-terminal Glu, and approximately opposite the lysine-rich site with the exposed heme edge.[13] In the crystal structure of the reduced protein, the thiol is slightly buried, but YCC nonetheless forms disulfide dimers upon oxidation. Proton NMR studies revealed that, although dimerization induces small changes at the heme site, this does not result in drastic structural disruption. The NMR spectrum of the dimer is similar to that of the monomer with a chemically modified Cys102.[14] The opposite, lysine-rich site has been shown to interact with the natural redox partners of cytochrome *c* to facilitate fast interprotein electron transfer. Its role in docking to yeast cytochrome *c* peroxidase (CCP),[15,16] the *bc*₁ complex,[17] and cytochrome *c* oxidase[18,19] has been demonstrated. Moreover, modification of Cys102 does not affect the binding and electron transfer to cytochrome *c* oxidase.[20]

Specific tethering of Cys102 to the electrode surface thus ensures a unique and functional orientation of YCC.[21] In this arrangement, the distance between the thiol and the buried edge of the heme is approximately 1.6 nm.[22] Because this is already close to the maximum distance for physiologically relevant electron tunneling rates,[23] an additional spacer between the electrode and Cys102 will render electron transfer severely rate limiting. Notably, Dutton and co-workers[9] found that YCC can be physisorbed on thiopropanol-modified gold, with the heme cleft facing solution. Upon coadsorption with cytochrome *c* oxidase, a stable complex was obtained that is active in oxygen reduction. However, even though the thiopropanol spacer is only 0.6 nm long, the authors found that electron relay through cytochrome *c* is rate limiting. This illustrates that direct binding of the cysteine thiol to the electrode surface is imperative. Ulstrup and co-workers achieved direct chemisorbtion of YCC on bare Au(111), and a low coverage of YCC was demonstrated by scanning tunneling microscopy.[24] However, only a very

weak, transient voltammetric signal of native YCC was observed due to unfolding of the protein. Bonanni and co-workers reported similar scanning probe measurements.[25] Although their cyclic voltammogram shows mostly native, adsorbed YCC, the very broad, asymmetrical peaks indicate extremely slow electron transfer.

In the present report, we demonstrate for the first time that YCC, directly chemisorbed on bare gold via Cys102, retains its native electron-transfer functionality. Vectorially immobilized YCC is highly stable, displays very fast interfacial electron transfer, and efficiently relays electrons to its natural partner cytochrome *c* peroxidase as well as to both *cd*₁ nitrite reductase and NO-reductase from *Paraccocus denitrificans*. Moreover, the immobilization procedure can be scaled down to interrogate zeptomole protein samples at a microelectrode.

Experimental Section

Materials. Iso-1-cytochrome *c* from the yeast *Saccharomyces cerevisiae* (YCC) was purchased from Sigma. Yeast cytochrome *c* peroxidase (CCP), expressed in *E. coli*, was a kind gift from Dr. M. Ubbink (Leiden University).[16] Crystals of CCP were dissolved in 20 mM sodium phosphate buffer (pH 6.1) with 80 mM NaCl, and the aliquots were stored at −80 °C until use. Nitric oxide reductase (NOR) and cytochrome *cd*₁ nitrite reductase (NIR) were purified from *Paracoccus denitrificans* Pd1222, grown anaerobically with nitrate as terminal electron acceptor, according to published methods.[26,27] Potassium nitrite (Fluka) solutions were freshly prepared, and hydrogen peroxide was diluted immediately before use from a new bottle (Sigma, 30%). Nitric oxide (NO) was added from a fresh stock solution of 100 μM, obtained by flushing anaerobic water with a 5% NO/95% N₂ gas mixture.[28] Deionized water (18 MΩ cm milli-Q, Millipore) was used to prepare all solutions and to rinse the electrodes.

Electrochemistry. A 10−25 μL droplet of solution was placed between the working electrode, the reference electrode, and a platinum wire counter electrode as described by Hagen.[29] The cell was flushed with wetted argon and connected to either an EcoChemie Autolab 10 potentiostat or to a Bioanalytical systems (BAS) CV-50W potentiostat. The step size of only 0.1 mV used by the latter in combination with low-pass filtering enables accurate determination of the surface coverage from the area under the voltammetric peaks.[30] For sub-nA current measurements, the BAS potentiostat was used in combination with a PA-1 preamplifier and a C-3 cell stand with Faraday cage. The working electrodes were gold disk electrodes (BAS) with diameters of 1.6 mm (2.0 mm²) and 5 μm (20 μm²), or a piece of gold foil with a wetted area of ∼15 mm². The reference electrode was either a saturated calomel electrode (SCE, Radiometer K-401), +244 mV versus the normal hydrogen electrode(NHE), or a Ag/AgCl/3 M NaCl electrode (BAS RE-5B), +215 mV versus NHE.

Prior to immobilization of cytochrome *c*, the gold surface was polished with a water-based diamond suspension (Buehler, 1 μm particles for the macroscopic electrodes, and 50 nm for the microelectrodes), rinsed, cleaned in 0.1 M H₂SO₄ by applying +1.6, −1.2, +1.6, and −1.2 V versus NHE for 60s each, and rinsed with water. Because in the oxidized, dimeric yeast cytochrome *c*, the surface cysteine is not accessible, the protein was reduced with dithiotreitol (DTT, Sigma) or tris[2-carboxyethyl]phosphine (TCEP, Pierce). Excess reductant was

(12) Baymann, F.; Barlow, N. L.; Aubert, C.; Schoepp-Cothenet, B.; Leroy, G.; Armstrong, F. A. *FEBS Lett.* **2003**, *539*, 91−94.
(13) Louie, G. V.; Brayer, G. D. *J. Mol. Biol.* **1990**, *214*, 527−555.
(14) Moench, S. J.; Satterlee, J. D. *J. Biol. Chem.* **1989**, *264*, 9923−9931.
(15) Pelletier, H.; Kraut, J. *Science* **1992**, *258*, 1748−1755.
(16) Worrall, J. A. R.; Kolczak, U.; Canters, G. W.; Ubbink, M. *Biochemistry* **2001**, *40*, 7069−7076.
(17) (a) Hunte, C.; Solmaz, S.; Lange, C. *Biochim. Biophys. Acta* **2002**, *1555*, 21−28. (b) Lange, C.; Hunte, C. *Proc. Natl. Acad. Sci. U.S.A.* **2002**, *99*, 2800−2805.
(18) Döpner, S.; Hildebrandt, P.; Rosell, F. I.; Mauk, A. G.; von Walter, M.; Buse, G.; Soulimane, T. *Eur. J. Biochem.* **1999**, *261*, 379−391.
(19) (a) Roberts, V. A.; Pique, M. E. *J. Biol. Chem.* **1999**, *274*, 38051−38060. (b) Flöck, D.; Helms, V. *Proteins* **2002**, *47*, 75−85.
(20) Kotlyar, A.; Borovok, N.; Hazani, M.; Szundi, I.; Einarsdóttir, Ó. *Eur. J. Biochem.* **2000**, *267*, 5805−5809.
(21) (a) Wood, L. L.; Cheng, S.-S.; Edmiston, P. L.; Saavedra, S. S. *J. Am. Chem. Soc.* **1997**, *119*, 571−576. (b) Edmiston, P. L.; Saavedra, S. S. *Biophys. J.* **1998**, *74*, 999−1006. (c) Edwards, A. M.; Zhang, K.; Nordgren, C. E.; Blasie, J. K. *Biophys. J.* **2000**, *79*, 3105−3117. (d) Tronin, A.; Edwards, A. M.; Wright, W. W.; Vanderkooi, J. M.; Blasie, J. K. *Biophys. J.* **2002**, *82*, 996−1003.
(22) Taking 1YCC (ref 13) as the starting point, reorientation of the three C-terminal amino acids Ala101, Cys102, and Glu103, avoiding overlapping van der Waals radii, results in a surface-exposed thiol at a distance of ∼1.6 nm from the buried heme edge. Experimentally, a distance >1.5 nm between the heme and a spin label attached to Cys102 has been found: Qu, K. B.; Vaughn, J. L.; Sienkiewicz, A.; Scholes, C. P.; Fetrow, J. S. *Biochemistry* **1997**, *36*, 2884−2897.
(23) Page, C. C.; Moser, C. C.; Chen, X.; Dutton, P. L. *Nature* **1999**, *402*, 47−51.
(24) (a) Hansen, A. G.; Boisen, A.; Nielsen, J. U.; Wackerbarth, H.; Chorkendorff, I.; Andersen, J. E. T.; Zhang, J. D.; Ulstrup, J. *Langmuir* **2003**, *19*, 3419−3427. (b) Zhang, J. D.; Grubb, M.; Hansen, A. G.; Kuznetsov, A. M.; Boisen, A.; Wackerbarth, H.; Ulstrup, J. *J. Phys.: Condens. Matter* **2003**, *15*, S1873−S1890.

(25) Bonanni, B.; Alliata, D.; Bizzarri, A. R.; Cannistraro, S. *ChemPhysChem* **2003**, *4*, 1183−1188.
(26) Girsch, P.; de Vries, S. *Biochim. Biophys. Acta* **1997**, *1318*, 202−216.
(27) Moir, J. W. B.; Baratta, D.; Richardson, D. J.; Ferguson, S. J. *Eur. J. Biochem.* **1993**, *212*, 377−385.
(28) Lide, D. L., Ed. *Handbook of Chemistry and Physics*, 81st ed.; CRC Press LLC: Boca Raton, FL, 2000.
(29) Hagen, W. R. *Eur. J. Biochem.* **1989**, *182*, 523−530.
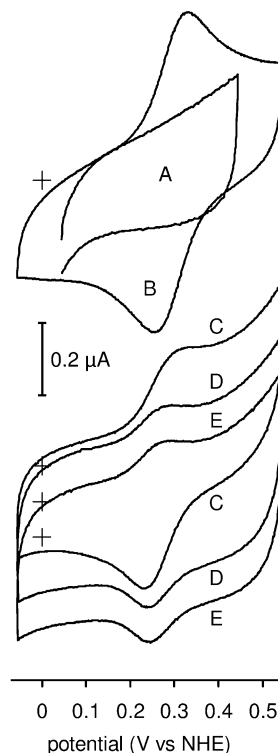(30) Heering, H. A.; Mondal, M. S.; Armstrong, F. A. *Anal. Chem.* **1999**, *71*, 174−182.

removed using a Biorad P6 microspin column. In the presence of $50-100$ μM reduced YCC, cyclic voltammograms were recorded between $+0.5$ and -0.1 V versus NHE with a 10 mV/s scan rate until a stable response was obtained. The electrode was subsequently rinsed with water, and a fresh droplet of buffer was applied. The buffer was $10-100$ mM potassium phosphate (KH_2PO_4 and K_2HPO_4 from Baker) or *N*-(2-hydroxyethyl) piperazine-*N*-(2-ethanesulfonate) (HEPES, Merck) at pH 7. A low surface coverage could also be obtained via 20 min of incubation of the gold electrode at open circuit with reduced YCC in 50 mM tris(hydroxymetryl)aminomethane (TRIS, ICN) buffer at pH 8.5, followed by thorough rinsing with water. Analysis of the noncatalytic peaks for adsorbed YCC was performed after subtracting a cubic splines background curve,[31] estimated by interpolation from the flanks of the peak. Control experiments with a solution of oxidized YCC were performed in the presence of 4,4′-dipyridyl (Sigma) as facilitator.[32]

Atomic Force Microscopy. Gold electrodes for AFM were made by evaporating approximately 250 nm gold on freshly cleaved mica (grade V-4, SPI supplies) that was degassed overnight at 400 °C and 10^{-7} bar prior to gold deposition. To obtain atomically flat gold(111) terraces, the gold was annealed in a hydrogen flame. A freshly annealed electrode was mounted in a custom-made 25 μL electrochemical cell with a flexible Ag/AgCl/saturated KCl reference electrode (FLEXREF from World Precision Instruments, $+199$ mV versus NHE) and a Pt wire as counter electrode. A rubber O-ring holding the mica/gold chip defines an electrode area of 7 mm². To preserve the Au(111) terraces, no further electrochemical cleaning was done on this type of electrode. Immobilization of cytochrome *c*, followed by rinsing the electrode and measuring the surface coverage in buffer, were done as described above, using the BAS potentiostat. After electrochemistry, the electrode was rinsed with filtered water, dried under a stream of nitrogen, and mounted in the AFM (Nanoscope IV, Digital Instruments). Images were recorded in the tapping mode, using silica cantilevers with a typical tip size of 10 nm (Olympus).

NIR Activity Measurements. The activity of NIR was measured in an anaerobic solution of 50 mM potassium phosphate at pH 7 with 10 mM ascorbate, 0.1 mM phenazine ethosulfate (Sigma), 0.1 mM reduced horse heart cytochrome *c* (Sigma), 10 mM KNO_2, and 5.6 nM of NIR. The production of NO was measured using a Clark electrode.[26] The activity was determined from the maximum slope, before the onset of NO-inhibition.

Results

Cytochrome *c* on Gold. As shown in Figure 1A, oxidized YCC does not give any response on a freshly cleaned, bare gold electrode. Only when a facilitator such as 4,4′-dipyridyl is added is a reversible, diffusion-controlled response obtained (Figure 1B). The midpoint potential of 290 mV versus NHE at pH 7 is close to the reported reduction potentials of YCC.[33,34] In contrast, a solution of reduced YCC without facilitator yields a reversible response with a midpoint potential of 268 mV (Figure 1C), reaching a maximum intensity after $2-5$ scan cycles ($4-10$ min). When this electrode is subsequently rinsed and brought into contact with buffer at pH 7 without protein, part of the

(31) Press, W. H.; Flannery, B. P.; Teukolsky, S. A.; Vetterling, W. T. *Numerical Recipes in Pascal*; Cambridge University Press: New York, 1989.
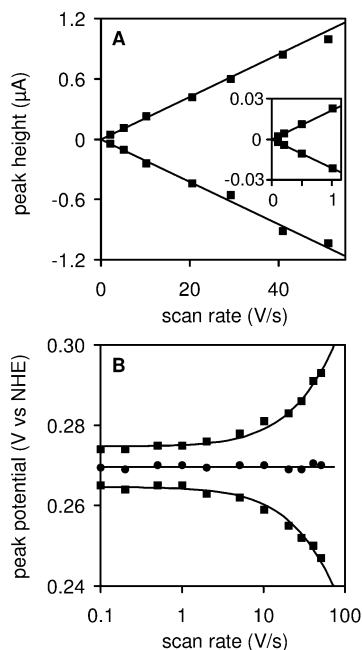(32) Eddowes, M. J.; Hill, H. A. O. *J. Chem. Soc., Chem. Commun.* **1977**, $771-772$.
(33) Terrettaz, S.; Chun, J.; Miller, C. J. *J. Am. Chem. Soc.* **1996**, *118*, $7857-7858$.
(34) (a) Rafferty, S. P.; Pearce, L. L.; Barker, P. D.; Guillemette, J. G.; Kay, C. M.; Smith, M.; Mauk, A. G. *Biochemistry* **1990**, *29*, $9365-9369$. (b) Davies, A. M.; Guillemette, J. G.; Smith, M.; Greenwood, C.; Thurgood, A. G. P.; Mauk, A. G.; Moore, G. R. *Biochemistry* **1993**, *32*, $5431-5435$. (c) Pollock, W. B. R.; Rosell, F. I.; Twitchett, M. B.; Dumont, M. E.; Mauk, A. G. *Biochemistry* **1998**, *37*, $6124-6131$. (d) Lett, C. M.; Guillemette, J. G. *Biochem. J.* **2002**, *362*, $281-287$.

Figure 1. Cyclic voltammograms of YCC on a bare gold electrode (area $\sim$15 mm²). (A) 100 μM oxidized YCC in 10 mM KPi, pH 7. (B) 100 μM oxidized YCC in 100 mM HEPES, pH 7, and 5 mM 4,4′-dipyridyl. (C) 50 μM reduced YCC in 10 mM KPi, pH 7 on bare gold. (D) The same electrode after rinsing, in 10 mM KPi, pH 7, without YCC. (E) 0.7 M KCl added. Traces C, D, and E are offset by -0.8, -0.9, and -1.0 μA, respectively, for clarity (the crosses indicate origins). The scan rate is 10 mV/s for all traces.

YCC response is still present (Figure 1D), indicating that the protein is adsorbed on the surface (cf. Figure 2). Upon addition of 0.7 M KCl, the response does not change (Figure 1E), showing that the adsorption is not electrostatic in nature. The YCC layer is remarkably stable: in many cases, some or all of the response is still observed after storing the electrode in pH 7 buffer for up to 48 h at 4 °C. The surface coverage, calculated from the area under the baseline-corrected peaks, ranges from 5% to 40% of a full monolayer (the crystallographic dimensions of 2.5×3.5 nm[13] yield 19 pmol/cm² for a densely packed monolayer), which is probably related to variations in surface cleanliness and roughness.

The scan-rate dependence of the heights and potentials of the peaks of a typical sample are plotted in Figure 2. Analysis of the baseline-corrected voltammograms by peak fitting yields an average width corresponding to $n = 0.99 \pm 0.08$ and an average integral of 2.20 ± 0.14 nC, which computes to 0.11 pmol/cm², or 6% of a monolayer. The proportionality of the peak heights to the scan rate (Figure 2A) confirms the adsorbed nature of YCC. Although a small peak separation is observed at low scan rates, additional broadening only occurs above 1 V/s (Figure 2B). A similar nonzero separation has also been observed for YCC, electrostatically adsorbed on indium/tin oxide.[35] Because this constant peak separation (termed "unusual quasi-reversibility", UQR, by Feldberg and Rubinstein[36]) is not

(35) El Kasmi, A.; Leopold, M. C.; Galligan, R.; Robertson, R. T.; Saavedra, S. S.; El Kacemi, K.; Bowden, E. F. *Electrochem. Commun.* **2002**, *4*, $177-181$.
(36) Feldberg, S. W.; Rubinstein, I. *J. Electroanal. Chem.* **1988**, *240*, $1-15$.

Figure 2. Scan rate dependence of YCC, chemisorbed on gold (2 mm²), in 50 mM KPi, pH 7. (A) Peak heights versus scan rate. The inset shows the data at low scan rates. The slopes of the lines correspond to the average peak height divided by scan rate of 21.2 ± 1.2 nC/V. (B) peak potentials E_p (■) and midpoint potentials (●) versus log scan rate. The solid lines are the peak potentials resulting from the Butler–Volmer equation with $\Delta E_p(0) = 10$ mV, $E^{\circ\prime} = 270$ mV, $k_0 = 1774$ s⁻¹ ($\alpha = 0.5$, $n = 1$, $T = 298$ K).
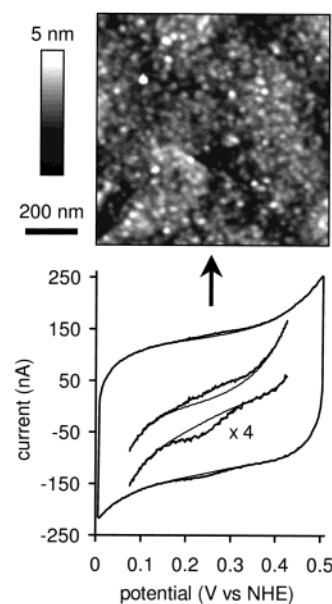
due to interfacial electron-transfer kinetics,[36–38] the rate constant for electron transfer between the gold surface and the heme is determined from the additional peak separation at high scan rates. The data are fitted to the peak potentials of simulated voltammograms,[30] using the Butler–Volmer equations to calculate the interfacial electron-transfer rate constants for reduction and oxidation:

$$k_{red} = k_0 \exp\{-\alpha nF(E - E^{0\prime})/RT\} \tag{1}$$

$$k_{ox} = k_0 \exp\{(1 - \alpha)nF(E - E^{0\prime})/RT\} \tag{2}$$

where k_0 is the standard rate constant, E is the applied potential, $E^{0\prime}$ is the equilibrium (midpoint) potential, α is the transfer coefficient, n is the number of electrons, F is the Faraday constant, R is the gas constant, and T is the temperature.[39] With $\alpha = 0.5$, $n = 1$, $T = 298$ K, this yields $k_0 = 1774$ s⁻¹, $E^{0\prime} = 270$ mV, and a low scan rate separation $\Delta E_p(\nu{\rightarrow}0) = 10$ mV. The midpoint potential of adsorbed YCC is close to that of YCC in solution. Because the reduction potential is extremely sensitive to the protein conformation and interactions between the surface and the lysine residues near the exposed heme edge,[10,40] this indicates that the heme edge is facing solution.

Figure 3 shows a voltammogram and corresponding AFM image of the same sample of YCC, chemisorbed on flame-annealed gold on mica. Features with an average height of 2.1

(37) Armstrong, F. A.; Camba, R.; Heering, H. A.; Hirst, J.; Jeuken, L. J. C.; Jones, A. K.; Léger, C.; McEvoy, J. P. *Faraday Discuss.* **2000**, *116*, 191–203.
(38) Jeuken, L. J. C. *Biochim. Biophys. Acta* **2003**, *1604*, 67–76.
(39) Bard, A. J.; Faulkner, L. R. *Electrochemical Methods: Fundamentals and Applications*, 2nd ed.; John Wiley & Sons: New York, 2001.
(40) Battistuzzi, G.; Borsari, M.; Sola, M. *Eur. J. Inorg. Chem.* **2001**, 2989–3004.

Figure 3. Tapping mode AFM (885 × 885 nm, 512 × 512 pixels, 5 nm z scale) of flame-annealed gold on mica with chemisorbed YCC (top) and cyclic voltammogram of the same sample (bottom) in 50 mM KPi, pH 7 (7 mm² exposed Au, 100 mV/s scan rate). The original data and 4-fold expanded data (minus an arbitrary slope for clarity) are plotted together with the estimated background used to determine the peak area.

± 0.5 nm and lateral dimensions (cross section widths) between 14 and 25 nm are observed on the Au(111) terraces. These features remain present after rinsing with water and are neither present on freshly annealed gold, nor on gold incubated with buffer only. The density of the features increases upon raising the applied YCC concentration. The observed heights are comparable to the height of 2.5 nm estimated from the crystal structure of YCC,[13] but the lateral dimensions suggest that the features are composed of multiple YCC molecules (assuming a tip width ≤14 nm). Approximately 650 features are counted per μm² in the AFM image, while the area under the voltammetric peaks is 5.9 nC. The peak area calculates to 61 fmol on an exposed geometric area of 7 mm², or 5300 molecules per μm² (i.e., 0.9 pmol/cm² or 5% of a fully packed monolayer). This implies that the observed features in the AFM image represent clusters of YCC, containing an average of approximately eight native, electrochemically active molecules. The stability of the samples during repeated AFM imaging, the observed height of the features, and uniformly fast electron transfer show that the clusters are monolayer islands of chemisorbed YCC.
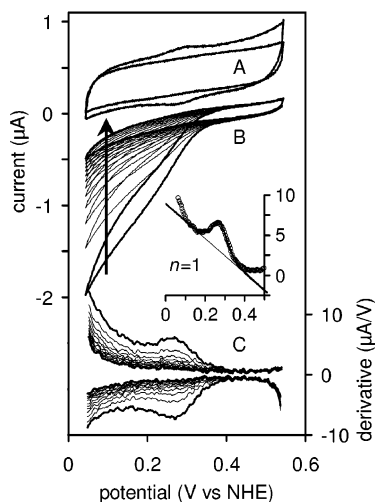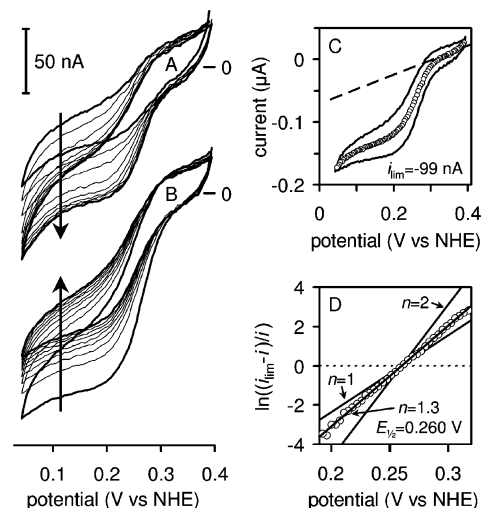
Catalytic Electron Transfer. To test the functionality that is expected for YCC, vectorially immobilized via Cys102, its capability to relay electrons to enzymes was investigated. Cytochrome *c* peroxidase (CCP) is one of the in vivo redox partners of YCC. When both CCP and hydrogen peroxide are added to the YCC-modified gold electrode, a clear reductive catalytic current is observed (Figure 4). The half-wave potential of the sigmoidal catalytic wave (267 mV at pH 7, 281 mV at pH 5.5) is close to the noncatalytic reduction potential of cytochrome *c*, and the slope of the wave corresponds to $n = 1.0$ (determined from the derivative peak, see inset of Figure 4). The catalytic current increases with the CCP concentration, sharply decreases upon addition of the CCP inhibitor NaF,[4,41] and is higher at pH 5.5 (>16 s⁻¹ per YCC) than at pH 7 (>6

Figure 4. YCC-modified gold electrode ($\sim$15 mm^2) with CCP. (A) In 100 mM HEPES pH 7 before and after catalysis (50 mV/s scan rate). Both voltammograms are offset by 0.4 μA for clarity. (B) In 80 mM Hepes pH 7 with 20 μM CCP and 8 mM H$_2$O$_2$; the bold lines are scans 1 and 13, scan rate is 10 mV/s. (C) Derivatives of (B) (cathodic sweeps are plotted with negative peaks). The inset shows the average derivative of the first cathodic and anodic sweep (symbols), and the fit to an $n = 1.0$ peak at 267 mV (bold line) with a linear baseline (thin line).

Figure 5. YCC-modified gold electrode ($\sim$15 mm^2) with NIR. (A) 76 μM NIR and 4.4 mM KNO$_2$ in 50 mM KPi pH 7. (B) Same electrode after rinsing, in 50 mM KPi pH 7 with 4.4 mM KNO$_2$ without NIR. Arrows indicate development with time (scan rate 5 mV/s); scans 1 and 9 are in bold. (C) Analysis of scan 1 from (B). The symbols are the average of the cathodic and anodic sweep; the dashed line is the estimated baseline. (D) Logarithmic plot of the average from (C) minus the baseline, with $i_{lim} = -99$ nA. The fitted line is for $n = 1.3$ and $E_{1/2} = 260$ mV. The $n = 1$ and $n = 2$ slopes are also shown.

s^{-1} per YCC) as expected from the pH-dependence of the enzyme activity.[42] When either YCC or CCP is absent, only the low-potential background due to direct reduction of H$_2$O$_2$ on gold is observed. These results show that H$_2$O$_2$ reduction is catalyzed by CCP and that YCC is properly oriented on the electrode to allow docking and electron transfer to CCP. However, the catalytic current and YCC coverage decrease with a half-life of around 2 min. With H$_2$O$_2$ present but no CCP, the YCC peaks decrease on a similar time-scale. The rate is first order in H$_2$O$_2$ ($k_1 = 0.54$ M^{-1} s^{-1}) with a half-life of 2.5 min in the presence of 8 mM H$_2$O$_2$. Moreover, when 4.8 mM H$_2$O$_2$ is added to 0.2 mM oxidized YCC and 5 mM 4,4′-dipyridyl in 0.1 M HEPES pH 7, the voltammetric response decays with a half-life of 4 min, with concomitant bleaching of the cytochrome *c* solution. Villegas and co-workers[43] reported that yeast cytochrome *c* is sensitive to oxidative damage by H$_2$O$_2$, causing both bleaching of the heme and oxidation of the cysteine to cysteic acid.

The more general applicability of the YCC-modified gold electrode has been explored by testing its ability to relay electrons to two key enzymes in the denitrification pathway of *Paracoccus denitrificans*, involved in the formation and reduction of nitric oxide. The soluble periplasmic cytochrome *cd*$_1$ nitrite reductase (NIR) catalyzed the one-electron reduction of NO$_2^-$ to nitric oxide (NO). This enzyme has 97.1% homology to the *cd*$_1$ NIR from *Paracoccus pantotrophus*,[44] which can use both cytochrome *c*$_{550}$ and pseudoazurin as electron donor and can also accept electrons from mitochondrial (horse heart) cytochrome *c*.[45] The next enzyme in the denitrification pathway is nitric oxide reductase (NOR), the membrane-bound cyto-

chrome *bc* complex that catalyzes the reduction of two NO to N$_2$O by cytochrome *c*$_{550}$ or pseudoazurin. In vitro, horse heart cytochrome *c* can also be used as electron donor.[46,47]

With a solution containing both NIR and nitrite, the YCC-modified gold electrode gives a reductive catalytic wave (Figure 5A). The maximum catalytic current increases with time until a stable maximum is reached ($i_{lim} = -65$ nA). When the electrode is rinsed and placed in a buffered nitrite solution without NIR (Figure 5B), the catalytic current is initially higher (-99 nA, Figure 5C) as compared to the last scans with NIR in solution, and decreases to a value that is comparable to the latter (-59 nA). This shows that NIR is firmly adsorbed, presumably on top of the cytochrome *c* layer. The initially higher turnover is most likely due to absence of NO inhibition, and the decrease is due to accumulation of NO near the surface rather than desorption of NIR. Control experiments in which either YCC, NIR, or nitrite is absent do not show catalytic activity, and addition of the inhibitor cyanide decreases the catalytic current (data not shown). The results clearly demonstrate that electrons are mediated to NIR by cytochrome *c*. As shown in Figure 5D, the half-wave potential is 260 mV, which is close to the YCC potential. However, the shape of the wave corresponds to a noninteger $n_{app} = 1.3$, which suggests cooperativity of the cofactors (cf. Discussion). With the area under the cytochrome *c* peak in buffer after recording trace B (34 nC = 0.35 pmol, or 2.4 pmol/cm^2, data not shown), the maximum catalytic current of -99 nA corresponds to a turnover rate of 2.9 s^{-1} per adsorbed cytochrome *c* molecule.

Upon addition of both NOR and nitric oxide to the YCC-modified gold electrode, a clear and very stable catalytic reduction current is observed (Figure 6A) with an $n = 1.0$

(41) Delauder, S. F.; Mauro, J. M.; Poulos, T. L.; Williams, J. C.; Schwarz, F. P. *Biochem. J.* **1994**, *302*, 437−442.
(42) Goodin, D. B.; Davidson, M. G.; Roe, J. A.; Mauk, A. G.; Smith, M. *Biochemistry* **1991**, *30*, 4953−4962.
(43) Villegas, J. A.; Mauk, A. G.; Vazquez-Duhalt, R. *Chem. Biol.* **2000**, *7*, 237−244.
(44) Baker, S. C.; Saunders, N. F. W.; Willis, A. C.; Ferguson, S. J.; Hajdu, J.; Fülöp, V. *J. Mol. Biol.* **1997**, *269*, 440−455.

(45) Richter, C. D.; Allen, J. W. A.; Higham, C. W.; Koppenhöfer, A.; Zajicek, R. S.; Watmough, N. J.; Ferguson S. J. *J. Biol. Chem.* **2002**, *277*, 3093−3100.
(46) Wasser, I. M.; de Vries, S.; Moënne-Loccoz, P.; Schröder, I.; Karlin K. D. *Chem. Rev.* **2002**, *102*, 1201−1234.
(47) Zumft, W. G. *Microbiol. Mol. Biol. Rev.* **1997**, *61*, 533−616.
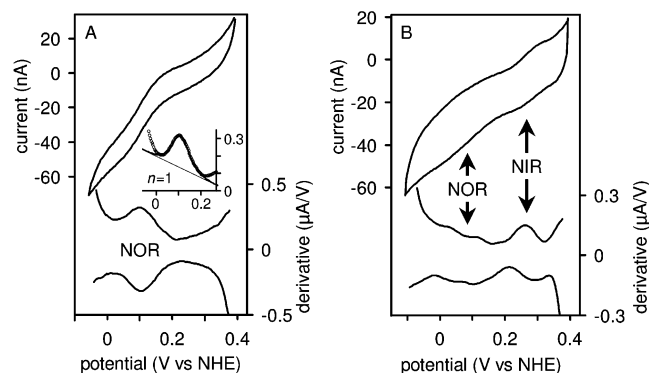
Figure 6. YCC-modified gold electrode ($\sim$15 mm^2) with NOR. (A) In 17 mM KPi pH 6 with 15 μM NOR and $\sim$5 μM NO; scan rate 1 mV/s. (B) 17 mM KPi pH 6 with 7 μM NOR, 19 μM NIR, and 34 mM KNO$_2$; scan rate 5 mV/s. The derivatives of the cathodic sweeps have negative peaks. The inset shows the average derivative of the cathodic and anodic sweep, and the fit to an $n = 1.0$ peak at 108 mV (bold line) with a linear baseline (thin line).

steepness and a half-wave potential of +108 mV (determined from the peak fit, see inset of Figure 6A), which is well below the reduction potential of YCC. No catalytic response is observed when either YCC, NOR, or NO is absent. Because the catalytic half-wave potentials with NIR and with NOR are well separated, it is possible to measure both enzymes simultaneously on the same electrode, and because the product of NIR is the substrate for NOR, it should be possible to observe NOR activity without adding NO. As shown in Figure 6B, with both NIR and NOR in solution but only nitrite as substrate, the two-step conversion of nitrite via nitric oxide to nitrous oxide is indeed observed. Interestingly, under these conditions, the NO reduction wave comprises two $n \approx 1$ sub-waves, clearly visible in the derivative, which points at a turnover mechanism involving multiple catalytic states or electron relay pathways in NOR.[2,3]

YCC and NIR on a Microelectrode. Mass transport to a large planar electrode occurs by linear diffusion, which is characterized by a decreasing flux with time ($\propto 1/\sqrt{t}$) and depletion of substrate. The turnover rate of NIR at the electrode could therefore be limited by diffusion. For the same reason, the formed product nitric oxide will accumulate near the surface and inhibit the enzyme (see Figure 5B). Contrarily, diffusion to a microelectrode is radial, which results in a steady-state flux proportional to the electrode radius.[39] Because the mass-transport limited current density (per area) increases with decreasing radius, smaller microelectrodes support higher enzymatic turnover rates. A 5 μm diameter disk electrode supports a diffusion-limited current of $I = 4nFDCr \approx 1$ nA for a substrate concentration $C = 1$ mM and a diffusion constant $D = 10^{-9}$ m^2/s.

Considering the dimensions of YCC,[13] a full monolayer on a 5 μm (20 μm^2) gold electrode consists of only $\sim$2.3 × 10^6 molecules (3.8 amol). Following the procedure to immobilize YCC that is the same as that used for macroelectrodes, and accumulating 100 scans at 20 mV/s scan rate, cytochrome c oxidation and reduction peaks can be detected with heights of 15 fA, on top of a capacitive electrode charging background current of $\sim$1 pA (Figure 7A). No such peaks are observed on untreated gold electrodes. After the estimated background was subtracted,[48a] the peaks are fitted to the theoretical shape for a reversible surface-confined one-electron redox process with an
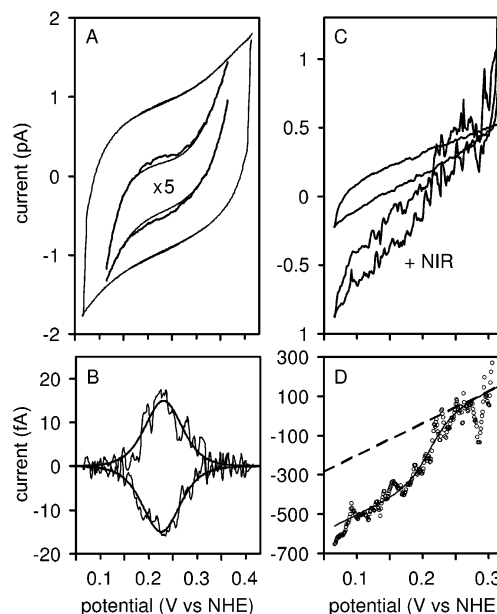
Figure 7. (A) YCC on a gold microelectrode (20 μm^2) in 50 mM KPi, pH 7; 20 mV/ s scan rate; 1.5 Hz filter; average of 100 cycles. The original data and five-fold expanded data (minus an arbitrary slope for clarity) are plotted together with the estimated background. (B) Baseline-corrected voltammogram, and fitted peaks: $E_m = 228$ mV, $\Delta E_p = 5$ mV, width = 89 mV ($n = 1$), height = 14.9 fA. (C) Sample from (A) before and after adding 10 mM KNO$_2$ and 10 μM NIR; 2 mV/s scan rate; 0.15 Hz filter, averages of 10 (without NIR) and 3 (with NIR) cycles. (D) Average of cathodic and anodic scans recorded with NIR minus those without NIR. The dashed line is the estimated residual slope. The solid line is the fitted sigmoidal ($E_{1/2} = 211$ mV, $n = 1.5$, $i_{lim} = -301$ fA) plus slope. The results are listed in Table 1 as experiment no. 1.

area of 77 fC. This computes to as little as 0.8 amol, which is less than 500 000 cytochrome c molecules and corresponds to a surface coverage of 4.0 pmol/cm^2 or 21% of a monolayer. Figure 7B shows that when NIR and nitrite are added to the solution, a catalytic current of 0.30 pA is observed.[48b] This corresponds to a nitrite turnover rate of 3.9 s^{-1} per adsorbed cytochrome c molecule in this experiment. The reproducibility of these experiments is demonstrated in Table 1. The average sample size is 0.65 amol (3.2 pmol/cm^2) or $\sim$390 000 YCC molecules. To our knowledge, these are by far the smallest samples detected by protein-film voltammetry to date. In the presence of NIR and nitrite, the average turnover rate per YCC molecule is 3.2 s^{-1}, and the slope of the wave yields $n_{app} \approx$ 1.4. These numbers are equal to those observed at macroscopic electrodes. However, both the noncatalytic midpoint potential and the catalytic half-wave potential are shifted as compared to the results on macroscopic electrodes, without affecting their shapes. A $\sim$40 mV downshift is reproduced with different batches of chemicals and different reference and 5 μm Au electrodes (experiments listed in Table 1). Test measurements with ferrocene derivatives in solution do not reproduce the shift, excluding impedance-related artifacts. Therefore, the lowered potentials most likely reflect a slightly altered environment.

(48) (a) Subtraction of a bare gold electrode blank is not sufficient for analysis because slight differences after polishing and cleaning yield differences in the background current that are relatively small, yet many times larger than the YCC peaks. (b) The voltammograms in the presence of enzyme and substrate are noisier as compared to the background. In part, this is expected because of the difference in the number of averaged traces (3 versus 10). Additional noise is probably generated by small fluctuations in the diffusion profile due to the long time-scale of the measurement.

Table 1. Summary of the Data with YCC Adsorbed on 5 μm Diameter Gold Electrodes (The Experiments in Which Both Noncatalytic and Catalytic Currents Are Measured Have Corresponding Numbers; Experiment No. 1 Is Plotted in Figure 7)

Noncatalytic (in 50 mM KPi, pH 7)

experiment[a]	E_m (mV)	ΔE_p (mV)	n_{app}[b]	height (fA)	area (fC)	coverage (amol)	molecules (10^5)
1 (A, I)	228	5	1.00	15	77	0.80	4.8
2 (A, I)	238	53	0.86	9	51	0.53	3.2
3 (A, I)	225	46	1.01	15	70	0.73	4.4
4 (A, I)	226	6	0.78	11	66	0.69	4.1
5 (B, I)	233	49	0.98	12	53	0.56	3.3
6 (B, I)	221	32	0.94	15	75	0.78	4.7
7 (B, II)	223	16	1.01	125[c]	45	0.47	2.8
Average	228	30	0.94	12.4[c]	62	0.65	3.9

Catalytic (10 μM NIR and 10 mM KNO$_2$ in 50 mM KPi, pH 7)

experiment[a]	$E_{1/2}$ (mV)	n_{app}	i_{cat} (fA)	turnover per YCC (s^{-1})
1 (A, III)	211	1.5	301	3.9
4 (A, IV)	198	1.4	226	3.4
7 (B, V)	201	1.2	65	1.4
8 (C, V)	213	1.5	246	4.0[d]
Average	206	1.4	210	3.2

[a] Three different electrodes have been used, labeled A, B, and C. The roman numbers are the measurement conditions: I, average of 100 scans at 20 mV/s with a 1.5 Hz filter; II, average of 100 scans at 250 mV/s and 50 Hz; III, average of 3 scans at 2 mV/s and 0.15 Hz; IV, average of 6 scans at 2 mV/s and 0.15 Hz; V, average of 3 scans at 2 mV/s and 0.5 Hz. [b] Noncatalytic n_{app} = 89/(peak width at half-height, in mV). [c] The average includes experiment 7, normalized to 20 mV/s (10 fA). [d] Turnover calculated using the average coverage of experiments 1−7 (0.65 amol).

Discussion

Cytochrome *c* Electrochemistry and Immobilization. Oxidized, dimeric YCC does not exchange electrons with a gold electrode unless the surface is modified with a facilitator like 4,4′-bipyridyl that promotes electron transfer to the positively charged heme edge. In contrast, when the bulk of YCC in solution is chemically reduced prior to voltammetry, a stable response rapidly develops without a facilitator. Because the exposed heme edge is equally accessible in both the oxidized (cystine) dimer and the reduced (cysteine) monomer, the response of reduced YCC is most likely due to the interaction between the exposed cysteine thiol and the gold electrode: reduced YCC is chemisorbed on the gold electrode, and this layer mediates electrons to cytochrome *c* in solution. When the excess cytochrome *c* is subsequently removed from solution, only the response of the adsorbed layer remains. The insensitivity of this response to high salt concentrations, the midpoint potential close to that of YCC in solution, and the ability to transfer electrons to YCC in solution, to CCP, NIR, and NOR, all indicate that YCC is covalently bound to gold via Cys102 and oriented with the accessible heme cleft toward solution.

Adsorption from a solution of reduced YCC is not only important to expose the thiol, but probably also prevents denaturation on the gold surface. NMR data have revealed that reduced YCC is substantially more rigid as compared to the oxidized species,[49] and EPR studies of spin-labeled Cys102 demonstrated more rapid temperature-induced unfolding of the

C-terminal region in the oxidized state.[50] Voltammetric cycling probably promotes chemisorption by creating a transient, local population of oxidized but monomeric YCC with a more flexible C-terminus. The stability of the chemisorbed YCC is almost certainly related to the observed tendency to form islands. The lateral confinement within such an island reduces its orientational freedom and thus prevents extensive direct contact between the protein and the gold surface.

Our results differ from those recently published by others. Ulstrup and co-workers[24] report that after 3 h of incubation of flame-annealed Au(111) with YCC, their in situ STM and voltammetric data show a low density overage with individual molecules, that are mostly unfolded. Bonanni and co-workers[25] reported very similar SPM data of YCC on gold. Although their voltammetric data show mostly native, adsorbed YCC, the coverage is much too high as compared to the SPM data and the peaks are highly asymmetric and very broad ($\sim$140 mV peak separation at a scan rate of 50 mV/s). This is symptomatic for very slow interfacial electron transfer: allowing for a large nonkinetic hysteresis of 50 mV, the remaining 90 mV compute to a k_0 of only 0.6 s^{-1}. This is more than 3 orders of magnitude slower than our measurements and suggests a separation between the heme and the gold of more than 2 nm (see below). This points at either multilayer adsorption or at least a very unfavorable orientation that does not involve a direct Cys102 to gold bond.

Interfacial Electron-Transfer Kinetics. According to the semiclassical model of Marcus,[51] the rate constant for nonadiabatic electron transfer between weakly coupled donor and acceptor sites at a fixed distance depends on the driving force (difference between the reduction potentials of donor and acceptor, E_D and E_A) and the reorganization energy λ, which is the energy (in eV) required to change the nuclear coordinates of the donor to those of the acceptor without transferring the electron:

$$k_{DA} = k_{max} \exp\left\{ -\frac{RT}{4\lambda F}\left[\frac{F}{RT}(E_D - E_A + \lambda)\right]^2 \right\} \qquad (3)$$

The electron-transfer rate constant increases with energy difference, reaching a maximum k_{max} when $E_D - E_A = -\lambda$, and decreases again at higher driving force (the inverted region). The preexponential factor k_{max} depends on the electronic coupling between the donor and acceptor. For long-range electron transfer from redox centers in proteins to a surface-bound acceptor, Gray and co-workers observed that k_{max} decreases exponentially with distance (*r*) between the donor and acceptor.[52] Extrapolated to van der Waals contact (0.36 nm), a common tunneling rate constant of $\sim$10^{13} s^{-1} was found for all systems:

$$k_{max} \approx 10^{13} \exp\{-\beta(r - 0.36 \text{ nm})\} \text{ s}^{-1} \qquad (4)$$

The decay constant β falls in the range of 8−16 nm^{-1}, depending on the nature of the protein matrix.[23,52,53]

(49) Barker, P. D.; Bertini, I.; Del Conte, R.; Ferguson, S. J.; Hajieva, P.; Tomlinson, E.; Turano, P.; Viezzoli, M. S. *Eur. J. Biochem.* **2001**, *268*, 4468−4476.

(50) Pyka, J.; Osyczka, A.; Turyna, B.; Blicharski, W.; Froncisz, W. *Eur. Biophys. J.* **2001**, *30*, 367−373.
(51) Marcus, R. A.; Sutin, N. *Biochim. Biophys. Acta* **1985**, *811*, 265−322.
(52) Gray, H. B.; Winkler, J. R. *J. Electroanal. Chem.* **1997**, *438*, 43−47.
(53) (a) Moser, C. C.; Keske, J. M.; Warncke, K.; Farid, R. S.; Dutton, P. L. *Nature* **1992**, *355*, 796−802. (b) Gray, H. B.; Winkler, J. R. *Annu. Rev. Biochem.* **1996**, *65*, 537−561. (c) Moser, C. C.; Page, C. C.; Chen, X.; Dutton, P. L. *J. Biol. Inorg. Chem.* **1997**, *2*, 393−398. (d) Winkler, J. R.; Gray, H. B. *J. Biol. Inorg. Chem.* **1997**, *2*, 399−404.

For application of eq 3 to electron transfer between an electrode at potential E and a redox center in the protein with reduction potential $E^{0'}$, all occupied (or vacant) states in the electrode must be considered as an electron donor (or acceptor).[39,54−56] The contribution of each state i at potential E_i can be estimated by multiplying the Marcus rate constant at driving force $E_i − E^{0'}$ by the probability that the state is occupied. For a metallic electrode, this probability is described by the Fermi−Dirac distribution $1/(1 + \exp(x))$ for a dimensionless potential difference $x = (E − E_i)F/RT$ from the applied potential E (i.e., the Fermi level). The total electron-transfer rate constant at given E is obtained by summing the contributions of all states:

$$k_{red/ox} = \frac{k_{lim}}{\sqrt{4\pi L}} \int \frac{\exp\{-(L \pm P - x)^2/4L\}}{1 + \exp(x)} \, dx \qquad (5)$$

where the dimensionless parameters $L = \lambda F/RT$ and $P = (E − E^{0'})F/RT$, and $L + P$ and $L − P$ apply to k_{red} and k_{ox}, respectively. The integration yields a sigmoidal dependence of the rate constant on applied potential, reaching a plateau[57]

$$k_{lim} = k_{max}\rho\frac{RT}{F}\sqrt{4\pi L} \qquad (6)$$

at high overpotential ($E − E^{0'} \ll −\lambda$ for reduction), and $k = {}^1/_2 k_{lim}$ at $E − E^{0'} = −\lambda$. As in eqs 3 and 4, k_{max} is the driving-force optimized Marcus rate constant for any single, fully occupied state, and ρ (in eV^{-1}) is the effective density of electronic states near the Fermi level. At small overpotentials relative to λ, eq 5 is indistinguishable from the Butler−Volmer eqs 1 and 2 with $\alpha = 0.5$.[55]

At the maximum scan rate of 51.2 V/s available with our equipment, the peak separation increases by as little as 37 mV (Figure 2B). This is much smaller than the reorganization energy of 0.61 eV found for diffusion-controlled reduction and oxidation of YCC on ω-hydroxythiol-modified gold at pH 7.[33,58] We therefore used the Butler−Volmer equation with $\alpha = 0.5$ to fit the data, yielding $k = 1774$ s^{-1} at $E = E^{0'}$. Substituting this and $\lambda = 0.61$ eV in eq 5 yields $k_{lim} = 4.0 \times 10^6$ s^{-1}, which is more than sufficient to drive even the fastest enzymes. With $\rho = 0.9/eV$,[59] eq 6 yields $k_{max} = 1.0 \times 10^7$ s^{-1}, which for a tunneling distance of 1.6 nm calculates to a decay constant of $\beta = 11.1$ nm^{-1} (eq 4). This shows that the direct covalent bond between gold and Cys102 provides efficient coupling between the heme and the electrode surface, consistent with the many through-bond sections between the heme and the C-terminus as seen in the crystal structure. For YCC, physisorbed on a thiopropanol monolayer with the heme cleft facing solution, Dutton and co-workers measured a standard rate constant k_0 of just 20 s^{-1}, ascribed to the additional 0.6 nm distance between the gold surface and the heme.[9] When cytochrome c oxidase is coadsorbed on this YCC layer, the catalytic oxygen reduction current is limited by electron relay through YCC. Because the rate of electron transfer from YCC to cytochrome c oxidase is $>10^4$ s^{-1},[20] the rate-limiting step seems to be the interfacial electron transfer. Evidently, direct chemisorption will remove this limitation and enable detailed mechanistic studies of intra- and interprotein electron-transfer processes.

A finite peak separation at low scan rates is regularly observed in protein-film voltammetry.[37] For both equine and yeast cytochrome c, electrostatically adsorbed on indium/tin oxide, Kasmi and co-workers report a limiting peak separation of around 10 mV and propose that this is due to a reversible, electron-transfer-induced conformational change.[35] However, a redox reaction coupled to a reversible chemical reaction will appear as a single, reversible net reaction at low scan rates, with peak separations approaching zero.[37,38] Instead, Feldberg and Rubinstein[36] propose an N-shaped free energy (potential versus charge) curve that results in a time-independent hysteresis equal to the free energy difference between the maximum and minimum of the curve. We postulate that such an N-shaped curve can be due to vibrational relaxation associated with the redox reaction. The observed minimum peak separations between 5 and 50 mV correspond to frequencies of $40−400$ cm^{-1}, a range that is dominated by protein conformational (collective mode) vibrations that are very important for electron transfer.[60] Moreover, a large number of YCC heme vibrational modes are found in this region.[61]

Electron Relay to Enzymes. The YCC-modified gold electrode mediates electrons to CCP from yeast, with a catalytic wave for the two-electron reduction of H_2O_2 to water centered close to the YCC redox potential. This differs markedly from CCP, directly adsorbed on a pyrolytic graphite edge electrode, for which the wave is centered close to the compound I redox potential of ~750 mV.[4,5] Clearly, the shift is due to slow interfacial electron transfer to YCC at such an unfavorably high potential: the reported[6] electrocatalytic turnover of 407 $H_2O_2/$ s^{-1} (814 e/s) at pH 5.4 is only matched by the interfacial electron-transfer rate to YCC below 309 mV (eq 5). Yet because this rate increases exponentially as the potential is lowered further, the shape and height of the catalytic wave will, although displaced, still reflect the properties of the YCC/CCP/H_2O_2 system. The observed $n = 1$ slope, despite the two-electron reaction that is catalyzed, suggests that the turnover rate is proportional to the fraction of reduced YCC and thus (at least in part) limited by the rate of electron transfer from YCC to CCP. In fact, for CCP on graphite, Heering et al. have found

(54) (a) Chidsey, C. E. D. *Science* **1991**, *251*, 919−922. (b) Chidsey, C. E. D. *Science* **1991**, *252*, 631.
(55) Honeychurch, M. J. *Langmuir* **1999**, *15*, 5158−5163.
(56) Adams, D. M.; Brus, L.; Chidsey, C. E. D.; Creager, S.; Creutz, C.; Kagan, C. R.; Kamat, P. V.; Lieberman, M.; Lindsay, S.; Marcus, R. A.; Metzger, R. M.; Michel-Beyerle, M. E.; Miller, J. R.; Newton, M. D.; Rolison, D. R.; Sankey, O.; Schanze, K. S.; Yardley, J.; Zhu, X. *J. Phys. Chem. B* **2003**, *107*, 6668−6697.
(57) Two major differences with the single donor−acceptor model are noted: because all levels contribute, the inverted regions of the individual levels are compensated and do not appear in the total rate constant. Furthermore, the reorganization energy is associated with the half-reaction of the redox center only, because the electrode does not contribute to it.
(58) For equine cytochrome *c*, electrostatically adsorbed with the heme cleft towards a carboxyl-terminated self-assembled monolayer on gold, Murgida and Hildebrandt reported that the reorganization energy is 0.22 eV, which is substantially lower as compared to that in solution due to exclusion of water: (a) Murgida, D. H.; Hildebrandt, P. *J. Phys. Chem. B* **2002**, *106*, 12814−12819. (b) Hildebrandt, P.; Murgida, D. H. *Bioelectrochem.* **2002**, *55*, 139−143. However, because in our system the heme cleft is facing the solution, we assume that the reorganization energy is equal to that of YCC in solution.

(59) For gold, the effective density of electronic states near the Fermi level is 0.3 eV^{-1} per atom (Papaconstantopoulos, D. A. *Handbook of the Band Structure of Elemental Solids*; Plenum Press: New York, 1986). Because the thiol sulfur most likely binds to three surface gold atoms (Tachibana, M.; Yoshizawa, K.; Ogawa, A.; Fujimoto, H.; Hoffmann, R. *J. Phys. Chem. B* **2002**, *106*, 12727−12736), we use $\rho = 0.9$ eV^{-1}, which is similar to the estimated $\rho = 1$ eV^{-1} for ferrocene-terminated alkanethiols studied by Chidsey (ref 54).
(60) (a) Xie, A.; van der Meer, L.; Austin, R. H. *J. Biol. Phys.* **2002**, *28*, 147−154. (b) Morita, T.; Kimura, S. *J. Am. Chem. Soc.* **2003**, *125*, 8732−8733.
(61) Zheng, J. W.; Ye, S. Y.; Lu, T. H.; Cotton, T. M.; Chumanov, G. *Biopolymers* **2000**, *57*, 77−84.

that reduction of compound II to Fe(III) is rate limiting due to gating by a coupled chemical step.[3] The decay of the catalytic H_2O_2 reduction current with CCP is caused by the instability of cytochrome c in the presence of H_2O_2, as reported by Villegas and co-workers.[43] Nevertheless, the initial catalytic response of the gold/YCC/CCP system proves that YCC is adsorbed with retention of its native electron-transfer activity.

The results demonstrate that chemisorbed YCC also mediates electrons to *Paracoccus denitrificans* nitrite reductase and that NIR is coadsorbed on the YCC layer. Comparison between the AFM and voltammetric data shows that YCC adsorbs in clusters of around eight molecules. Using the crystallographic dimensions of YCC,[13] such monolayer islands have diameters of ∼9 nm. Because the crystal dimensions of the *Paracoccus pantotrophus* NIR dimer are 5 nm × 10 nm (and 6 nm "high", from the perspective of the c-domains),[62] only one NIR dimer is likely to find a favorable docking position per YCC island. This implies that as little as 80 zmol (∼49 000 molecules) of NIR is coadsorbed on the average 0.65 amol (∼390 000 molecules) of YCC at the 5 μm electrodes. The average electrocatalytic activity of 3.2 s^{-1} per YCC thus yields an estimated turnover of 26 s^{-1} per NIR dimer, or 12.5 U/mg. This is comparable to the specific activity of 13.6 U/mg, measured at pH 7 in the presence of saturating concentrations of reduced cytochrome c and nitrite. The turnover per YCC is equal on macroscopic and microelectrodes, although linear diffusion to the former should cause substrate depletion. The equality can be explained by the topography of the YCC layer: because NIR does not exchange electrons with bare gold, the ensemble of islands acts as an array of nanoelectrodes, allowing more efficient mass transport.

The turnover rate of NIR is much lower than the interfacial electron transfer to YCC (k_0), but the half-wave potential of the catalytic wave is slightly lower than the midpoint potential of YCC. Although this might suggest that the turnover is limited by the fraction of reduced YCC and thus by interprotein electron transfer, the $n_{app} = 1.4$ slope of the wave is clearly at odds with this. Therefore, electron relay through YCC is not rate limiting, and both the wave shape and the potential reflect the properties of the heme centers of NIR. For the one-electron reduction of nitrite to nitric oxide, catalyzed by a one-electron redox center (d_1 heme), an $n \leq 1$ Nernstian sigmoidal catalytic wave should be expected. Consequently, the $n > 1$ catalytic wave is indicative of positive cooperativity between the heme groups, either within or between the NIR subunits, or between YCC and NIR. For the related *Paracoccus pantotrophus* NIR, positive cooperativity is observed between hemes c and d_1 within one subunit.[63] Titration curves with $n_{app} = 1.4$ are found at 20 °C, increasing to fully $n = 2$ at higher temperature with an equilibrium potential of 140 mV. The one-electron-reduced intermediate state cannot be obtained unless NIR is depleted of the d_1 heme. The authors suggest that this cooperativity is due to coupling of the redox states of hemes c and d_1 via the connected ligands His17 and Tyr25 of oxidized c and d_1, respectively, that are exchanged for Met106 and released upon reduction of the respective hemes. *Pseudomonas aeruginosa cd_1* NIR has more tightly intertwined subunits as compared to

Paracoccus pantotrophus NIR, and the heme sites within each subunit do not cooperate. Instead, a positive allosteric cooperativity of 30 mV has been observed between the two d_1 hemes and an equal negative cooperativity between the c hemes, resulting in a titration curve with a slope of $n = 1.6$.[64] In contrast, the cd_1 NIR from *Pseudomonas stutzeri* exhibits negative allosteric cooperativity between the two d_1 sites.[65] With the YCC electrode, it may be possible to clarify whether the cooperativity in *P. denitrificans* NIR is allosteric or not.

Chemisorbed YCC is also able to relay electrons to *Paracoccus denitrificans* NOR. Notably, the half-wave potential for electrocatalytic NO reduction of +108 mV at pH 6 is much lower than the YCC equilibrium potential and is in fact close to the reduction potential of the high-spin heme b_3 in the active site (+62 mV at pH 7, +20 mV at pH 8.5).[66] Reduction of YCC by the electrode is not rate limiting: the interfacial electron transfer to YCC is 3×10^4 s^{-1} at $E = 108$ mV (eq 5), as compared to the reported k_{cat} of 200 NO/s.[46] The catalytic wave is not centered at the redox potential of YCC, which means that the turnover is not proportional to the fraction of reduced YCC and thus that interprotein electron transfer is also not limiting. The fact that the applied potential must be close to the heme b_3 redox potential for turnover signifies the importance of the fully reduced heme b_3 Fe(II)/Fe$_B$(II) active site in the mechanism, as proposed by de Vries and co-workers.[46,67] The $n = 1$ steepness of the catalytic wave reflects the rate-limiting reduction of heme b_3 via the high-potential centers in NOR ($E_{m(pH7.6)} = +345$ mV for LS heme b, +310 mV for LS heme c, and +320 mV for Fe$_B$[66]), which in turn are rapidly reduced by YCC ($E_m = +270$ mV). Interestingly, the lower catalytic half-wave potential of NOR as compared to that of NIR makes it possible to measure the activities of both enzymes on the same electrode. This is advantageous, not only to study the interaction between the enzymes, but potentially also for simultaneous sensing of nitrite and nitric oxide.

Conclusions

We have demonstrated that cytochrome c from yeast, chemisorbed directly on a gold electrode, is stable and retains its native redox potential and electron-transfer functionality. The bond between Cys102 and the gold surface allows for very fast interfacial electron transfer to the heme, and at the same time ensures an orientation that is favorable for functional docking of redox enzymes. The ability to relay electrons to CCP, NIR, and NOR clearly illustrates the versatility of the system. Although a detailed analysis of the catalytic properties of each of these systems is beyond the scope of this paper, some tentative conclusions can already be drawn: (1) The turnover of CCP is, at least partially, limited by electron transfer between YCC and CCP. (2) The catalytic wave shape with NIR shows positive cooperativity between the cofactors. (3) The catalytic activity of NOR depends on the redox state of the active site

(62) Fulop, V.; Moir, J. W. B.; Ferguson, S. J.; Hajdu, J. *Cell* **1995**, *81*, 369–377.

(63) Koppenhöfer, A.; Turner, K. L.; Allen, J. W. A.; Chapman, S. K.; Ferguson, S. J. *Biochemistry* **2000**, *39*, 4243–4249.

(64) Blatt, Y.; Pecht, I. *Biochemistry* **1979**, *18*, 2917–2922.

(65) Farver, O.; Kroneck, P. M. H.; Zumft, W. G.; Pecht, I. *Proc. Natl. Acad. Sci. U.S.A.* **2003**, *100*, 7622–7625.

(66) (a) Grönberg, K. L. C.; Roldán, M. D.; Prior, L.; Butland, G.; Cheesman, M. R.; Richardson, D. J.; Spiro, S.; Thomson, A. J.; Watmough, N. J. *Biochemistry* **1999**, *38*, 13780–13786. (b) Field, S. J.; Prior, L.; Roldan, M. D.; Cheesman, M. R.; Thomson, A. J.; Spiro, S.; Butt, J. N.; Watmought, N. J.; Richardson, D. J. *J. Biol. Chem.* **2002**, *277*, 20146–20150.

(67) (a) Moënne-Loccoz, P.; de Vries, S. *J. Am. Chem. Soc.* **1998**, *120*, 5147–5152. (b) Moënne-Loccoz, P.; Richter, O. M. H.; Huang, H. W.; Wasser, I. M.; Ghiladi, R. A.; Karlin, K. D.; de Vries, S. *J. Am. Chem. Soc.* **2000**, *122*, 9344–9345.

heme b_3. These examples demonstrate that, due to the very fast interfacial electron transfer and proper vectorial orientation, redox enzymes can be interrogated electrochemically via YCC, thus significantly extending the applicability of protein-film voltammetry to enzymes that cannot directly communicate with an electrode. The feasibility to miniaturize the system to sub-attomole samples offers great potential for applications in microscopic biosensor devices and multi-enzyme arrays. Direct immobilization of native cytochrome c on gold(111) terraces and coadsorption of enzymes open the way to detailed scanning probe microscopy studies of redox protein complexes.